Influence of Gap Size and Dielectric Constant of the Packing Material on the Plasma Behaviour in a Packed Bed DBD Reactor: A Fluid Modelling Study

Koen Van Laer,* Annemie Bogaerts

A packed bed dielectric barrier discharge (DBD) was studied by means of fluid modelling, to investigate the influence of the dielectric constant of the packing on the plasma characteristics, for two different gap sizes. The electric field strength and electron temperature are much more enhanced in a microgap reactor than in a mm-gap reactor, leading to more current peaks per half-cycle, but also to non-quasineutral plasma. Increasing the dielectric constant enhances the electric field further, but only up to a certain value of dielectric constant, being 9 for a microgap and 100 for a mm-gap reactor. The enhanced electric field results in a higher electron temperature, but also lower electron density. This last one strongly affects the reaction rate.

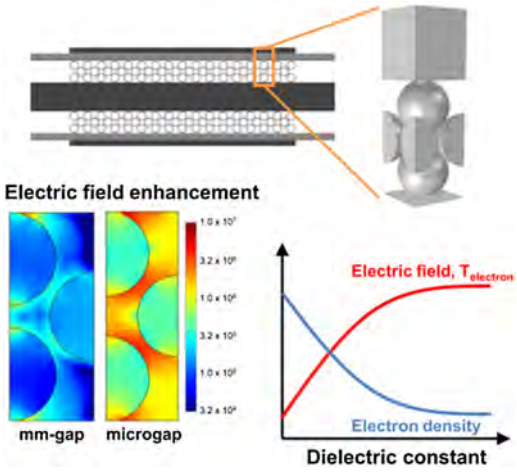

1. Introduction

Packed bed dielectric barrier discharge (DBD) reactors have received a lot of attention in recent years for environmental applications, such as for gaseous pollutant removal (e.g. NOx, VOC, . . .) or for gas conversion.[1–10] Indeed, introducing a packing in a DBD reactor was found to enhance the energy efficiency of the process, or, if the packing is catalytically active, even to steer the process towards a certain preferred end product, in so-called plasma catalysis.[11–12] The underlying mechanisms of plasma catalysis are, however, not yet fully understood. One of the problems in plasma catalysis is that dielectric effects (from the dielectric constant (ε) of the packing beads) and chemical catalytic effects (either due to the beads themselves or from the catalytically active coating on the beads) take place at the same time, influencing each other during the discharge. Since these effects cannot be easily distinguished, it is of great importance to first study the dielectric effect of the packing material itself, before adding a catalytic coating on the beads.

The problem with introducing any packing material in a DBD reactor is that experimental plasma diagnostics become more difficult. The plasma formation and propagation are more defined by local effects, such as the influence of contact points on the electric field and electron temperature. The importance of these effects also depends on the location in the reactor. In addition, the packing is also blocking visibility for optical diagnostics. A computational study can therefore, be very interesting, to achieve a better

K. Van Laer, A. Bogaerts
Research Group PLASMANT, Department of Chemistry, University of Antwerp, Universiteitsplein 1, 2610 Wilrijk-Antwerp, Belgium
E-mail: koen.vanlaer@uantwerpen.be

understanding of the effect of packing beads on the discharge behaviour.

The number of numerical studies on packed bed DBD reactors is however, rather limited. Chang and Takaki et al. developed a simplified time-averaged 1D numerical plasma model for N_2, based on solving Poisson's equation and transport equations.[13,14] They found that all plasma parameters increase upon increasing applied potential and dielectric constant. Due to the 1D limitation, the void between the beads was assumed to be spherical. Kang et al. developed a 2D model of a DBD reactor with two stacked ferroelectric beads inside, studying the propagation of the microdischarges in the first 20 ns.[15] Russ et al. used a 2D fluid model to simulate transient microdischarges in a packed bed DBD reactor filled with dry exhaust gas ($N_2/O_2 = 80/20$ and 500 ppm NO).[16] The work was limited to a short 1D discharge with a constant applied potential. Although not directly applied to a packed bed reactor, Babaeva et al. performed very relevant modelling work on the influence of dielectric spheres blocking a plasma streamer, using a 2D fluid model in humid air ($N_2/O_2/H_2O = 79.5/19.5/1$).[17]

Recently, within our group PLASMANT, two different modelling studies were performed on packed bed DBD reactors.[18,19] The first study involved a 2D particle-in-cell/Monte Carlo collision (PIC/MCC) model to describe the filamentary discharge behaviour in a packed bed DBD reactor in air ($N_2/O_2 = 80/20$).[18] The second study used two different axisymmetric 2D fluid models to simulate the initiation and propagation of a helium discharge at low and higher applied potential.[19] These two complementary axisymmetric models (or geometries) each focussed on a specific characteristic feature of a packed bed plasma reactor. The first model considered a physical contact point between the beads, while the second model focussed on the connection between the void spaces. It was found that the discharge was always initiated at the position where the electric field and electron temperature are the highest, which is near the physical contact points. For studies of a few cycles of applied potential, the second model is better suited, because its geometry is closer to reality, with dielectric material blocking the open gas gap. These studies revealed that at sufficiently high applied potential the discharge is able to spread across the gas gap, travelling through the 'channels' that connect the voids.

In the present paper, we make use of this second model, i.e. the so-called 'channel of voids' 2D axisymmetric model, to elucidate the pure dielectric effect of the packing beads in a packed bed DBD reactor, by investigating the influence of the dielectric constant of the packing material on the plasma behaviour in a helium discharge.[19] In addition, we study the influence of the gas gap size on the dielectric packing effect, by comparing a normal mm-gap and a so-called microgap. Indeed, it has been suggested by Duan et al. that a packed bed DBD microplasma yields promising conversions and energy efficiencies for CO_2 splitting, in the same order, if not better than in a normal size reactor.[20] The maximum achievable conversion in this microreactor setup was reported to be 41.9% for a packing of CaO, with an energy efficiency of 5.7%, while to our knowledge, the highest conversion reported in a normal size packed bed DBD reactor was very comparable, namely 42% with a zirconia packing, but the corresponding energy efficiency was slightly lower, i.e. 4.7%.[11] However, these results are not directly comparable since they use different packing materials. Moreover, the CO_2 capturing abilities of CaO can influence the results. In principle, a better comparison can only be made when the same packing material is used in both a microgap and mm-gap reactor. For γ-Al_2O_3, the maximum obtained CO_2 conversion reported for a microgap reactor is 16.3%, with an energy efficiency of 4.5%,[20] while in a mm-gap reactor, a comparable conversion of 16.0% could only be reached with a somewhat lower energy efficiency of 3.8%.[8] A plasma is called a microplasma when it is confined to critical dimensions below approximately 1 mm.[21] The smaller space in a microreactor implies a stronger electric field, and therefore, a higher energy density. We will thus, compare two different reactors, one large reactor with a gas gap of 4.5 mm and one microreactor with a gap of 0.5 mm. These reactors will be packed with different types of dielectric material, covering a wide range of dielectric constants, from 5 (glass, quartz) over 9 (alumina), 25 (zirconia) and 100 (titania), up to 1000 (barium titanate). The ratio of bead size over gap size will be kept constant in this study. In the future we will investigate the influence of the bead size with constant gap size. Note that the actual size of the gas volume can be estimated to be close to 26% of the total volume, which would be the case if the packing fills the void space perfectly, as stated by the Kepler conjecture.

2. Model Description

The 2D axisymmetric fluid model is developed with the built-in plasma module of the multiphysics software package COMSOL (version 5.0).[22] The model is based on solving a set of coupled differential equations that express the conservation of mass, momentum and energy, for the different plasma species. The Poisson equation is also solved to self-consistently calculate the electric field distribution based on the freshly calculated charged species densities at each time step. For a more

detailed explanation about the equations solved, we refer to our previous paper.[19]

The investigated 2D axisymmetric geometry, both for the mm-gap and the microgap reactor, is based on the concept of a 3D unit cell of a packed bed DBD reactor, shown in Figure 1. The stacking of the beads is based on a face-centered cubic formation, but since the combination of the gap size and the bead diameter is not perfect, the top and bottom bead are a little bit closer to each other, creating some spacing between the four beads in the middle plane. To solve the model entirely in 3D would require calculation times of several months. The 2D axisymmetric geometry uses several smart approximations to give the best possible representation of the real 3D geometry. More specifically, the 3D reactor has two characteristic features: the contact points between the dielectric beads and a connection between the void spaces in between the beads, i.e. a so-called 'channel of voids'. The contact points between the dielectric materials will have a large influence on the electric field distribution inside the reactor, due to polarisation of the dielectric beads, caused by the applied potential difference between the powered and grounded electrode. However, our previous study illustrated that the electric field enhancement obtained with a model considering no contact between the beads (like in the 2D geometry shown in Figure 1) was very similar to the results of a model with contact points, thus, justifying the use of the geometry shown in Figure 1.[19] In addition, the contact points between the beads also create a direct connection between the grounded and powered electrode through the dielectric material. This direct connection has the ability to lower the electric field strength over the entire gap. However, we performed 2D and 3D electrostatic simulations (i.e. not including any plasma reactions), and the results indicated that the influence of this connection is only minor. On the other hand, the connection of the void spaces between the beads was found to be crucial for a correct representation of the real geometry, and to account for this, the dielectric beads need to be separated from each other. Hence, this explains our choice of using the 2D geometry. The channel width in this 2D model is based on the diameter of the enclosed sphere that fits in the gap between three touching beads in the real 3D geometry. Note that in Figure 1, the rotational axis is positioned on the left side of the geometry, so the beads on the right will actually have a torus-shape after rotation, which of course does not reflect the reality. However, we believe that the latter will have a minor effect on the plasma behaviour near the contact points and in the voids between the beads, and since we are limited to a 2D model, we believe that this geometry is the best possible approach.

As mentioned in the Introduction, the model is applied to a helium plasma. The reaction set consists of 23 reactions between six different species, i.e. electrons (e), neutral helium atoms (He), positive helium atomic and molecular ions (He^+, He_2^+), metastable helium atoms, He(2^1S) and He(2^3S), which are combined into one effective level He^* and helium dimers (He_2^*). The complete reaction set, including the rate coefficients, as well as the information about the transport coefficients of the species, can be found in our earlier paper.[19]

The packing beads and dielectric layer are considered to be smooth solid objects without any surface roughness or porosity. They are treated with conservation of charge inside and charge accumulation on the surface. At the walls several surface reactions are taken into account: quenching of helium atomic and molecular metastables and electron-ion recombination of He^+ and He_2^+ ions to ground state helium atoms, with a probability of 0.05 to emit a secondary electron with energy of 5 eV, considered to be the same for all different packing materials. The outer boundary on the right side of the geometry is treated with an insulation boundary condition, setting the normal fluxes of electrons and electron energy on this boundary to zero, and a zero charge boundary condition, defining the normal electric displacement field equal to zero. This combination implies periodicity with a normal zero gradient of charged species across the boundary. The upper electrode is powered with a radio frequent applied potential of 7.5 kV peak-to-peak, while the lower electrode is ground (0 V). The pressure is kept constant at 1 atm, and the temperature is fixed at 300 K.

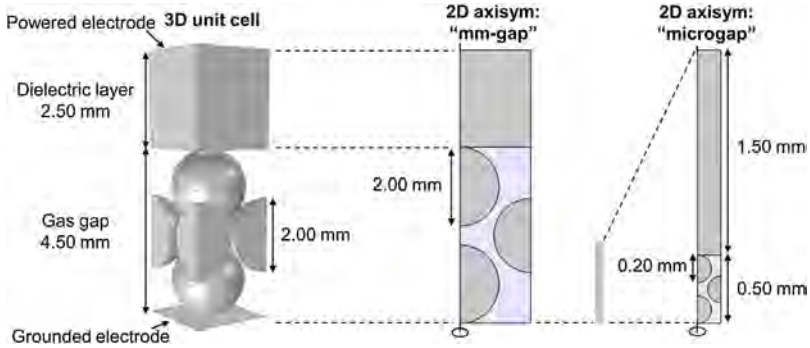

Figure 1. 3D unit cell of the packed bed DBD reactor, and 2D axisymmetric geometry, used to mimic the packing effect, with dimensions indicated for both the mm-gap and the microgap reactor.

3. Results and Discussion

3.1. Influence of the Gap Size

To illustrate the influence of the gap size on the discharge behaviour, the results

for both a large gap of 4.5 mm (mm-gap) and a smaller gap of 0.5 mm (microgap) are compared for the same packing with $\varepsilon = 25$ and the same applied potential of 7.5 kV_{ptp}. First, we take a look at the current profiles over one cycle of applied potential, as illustrated in Figure 2. Note that to calculate the current, the size of the electrode surface has to be known. In the model, this is the size of the circle formed by rotating the grounded electrode around the axis of symmetry. However, to make the modelling results representative for a full reactor and comparable with experiments, the current values are multiplied by a factor that represents the ratio between the real electrode surface and the modelled circle. The real electrode surface is calculated from the cylindrical geometry, found in a previous publication.[11] Because it is a cylindrical DBD reactor, the top and bottom surface (or more specifically, the surface area of the outer and inner cylindrical electrodes) will not be exactly the same, and therefore, the average is taken. The microgap reactor is assumed to be formed with the same dielectric (alumina) tube (i.e. the same inner diameter), but with an inner electrode with much larger diameter than for the mm-gap reactor, reaching a gap of 0.5 mm.

The discharge in the mm-gap reactor is characterised by a few current peaks per half cycle, shown by Figure 2(a). The first three peaks are caused by local discharges, which are found in between the beads on the left (1), at the contact point of the top bead with the dielectric layer (2) and above and below the bead on the right (3), respectively (see the inset in Figure 2). The fourth and strongest current peak comes from a discharge spreading over the full height of the gas gap, travelling through the channels that connect the voids. This was illustrated in our previous paper.[19] The maximum values of electron density and total ion density are comparable here; in other words, the plasma is more or less quasineutral. However, near the walls the electron density will be lower, due to sheath formation.

In the microgap reactor, the discharge behaviour is totally different. Figure 2(b) shows that the same applied potential yields much more current peaks per half cycle, and they are also up to a factor 4 higher than in the mm-gap reactor. These current peaks are coming from consecutive discharges taking place in the void spaces between the two beads on the left, and above and below the bead on the right. The discharge no longer travels through the gaps between the beads, but stays localised in the voids.

The following time-averaged 2D plots are constructed by averaging over 200 individual results per cycle of applied potential, i.e. an output every 2×10^{-7} s. This is sufficiently small since in helium, no short lived filamentary discharge behaviour is expected, that would negatively affect the averaging. From Figure 3, it is clear that the time-averaged electric field in the microgap reactor is much higher than in the mm-gap reactor, especially in the channels between the voids (i.e. up to 10^7 V m^{-1} in the microgap vs. 6.5×10^6 V m^{-1} in the mm-gap reactor). As a result, the critical electric field strength to create a breakdown in the gas is more often reached in the microgap reactor, thus, resulting in much more current peaks per half cycle of applied potential.

The 2D electron temperature profile in Figure 4 looks very similar to the electric field distribution. When the electric field is strong, the electrons are accelerated more, leading to an enhanced electron temperature. Therefore, the maximum values of electron temperature will also be found near the contact points and in the channels between the voids, where the beads are the closest to each other. In general, the electron temperature is again much higher

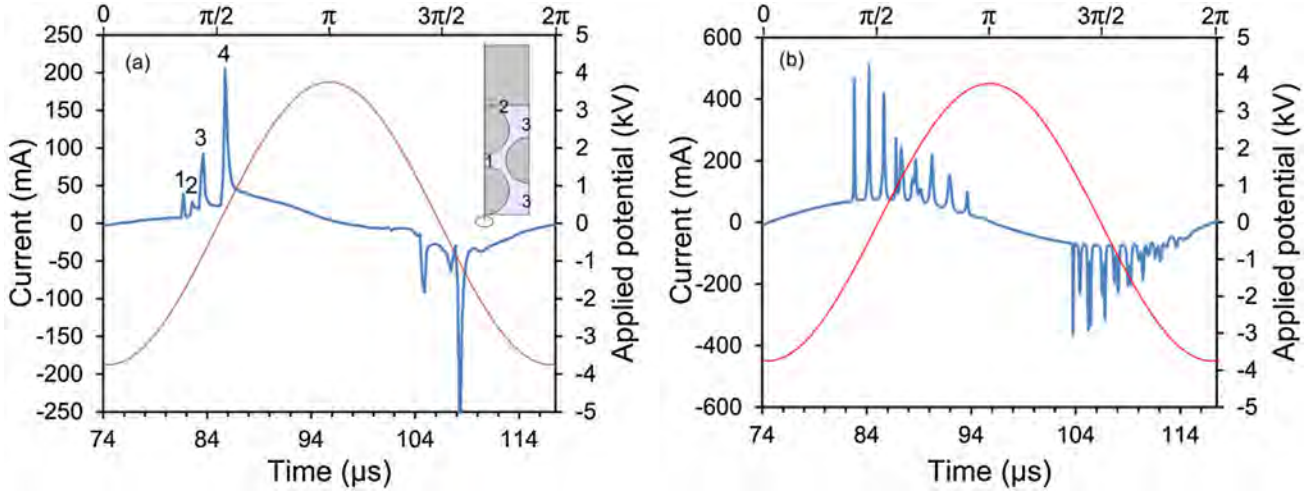

Figure 2. Current profiles of the mm-gap (a) and microgap (b) packed bed DBD reactors with a zirconia packing, for one cycle of applied potential.

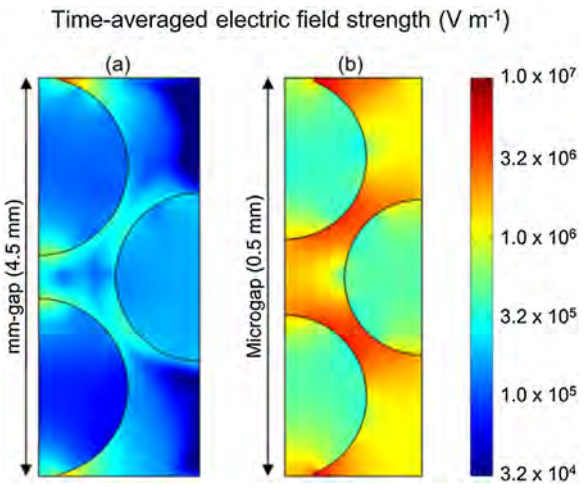

Figure 3. Time-averaged electric field strength of the mm-gap (a) and microgap (b) reactors with a zirconia packing ($\varepsilon = 25$), for one cycle of applied potential.

in the microgap reactor, with values up to 11 eV at the contact points and in the channels between the voids, and in the order of 6 eV in the voids, while in the mm-gap reactor, the electron temperature is only around 3 eV in the voids, rising up to 6 eV in the channels between the voids, and up to 9 eV at the contact point between the upper beads and the dielectric layer. This difference directly arises from the higher electric field strengths in the microgap DBD reactor, shown in Figure 3.

The time-averaged electron and total ion density profiles in Figure 5 show that the maximum plasma density in the microgap reactor is spread out more evenly over the different void spaces, whereas for the larger reactor the most intense plasma is located in a thin area directly above and below the center of the bead on the right. Close to

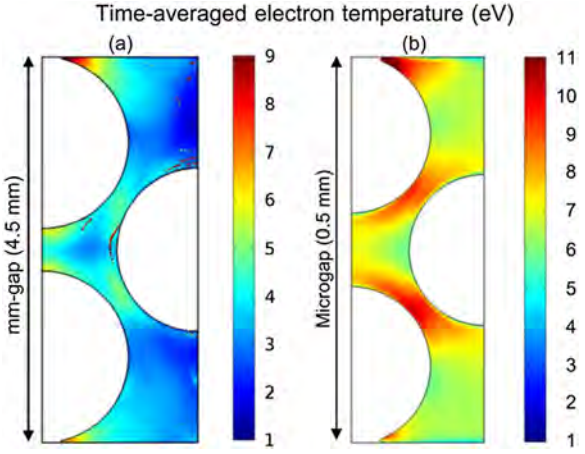

Figure 4. Time-averaged electron temperature of the mm-gap (a) and microgap (b) reactors with a zirconia packing ($\varepsilon = 25$), for one cycle of applied potential.

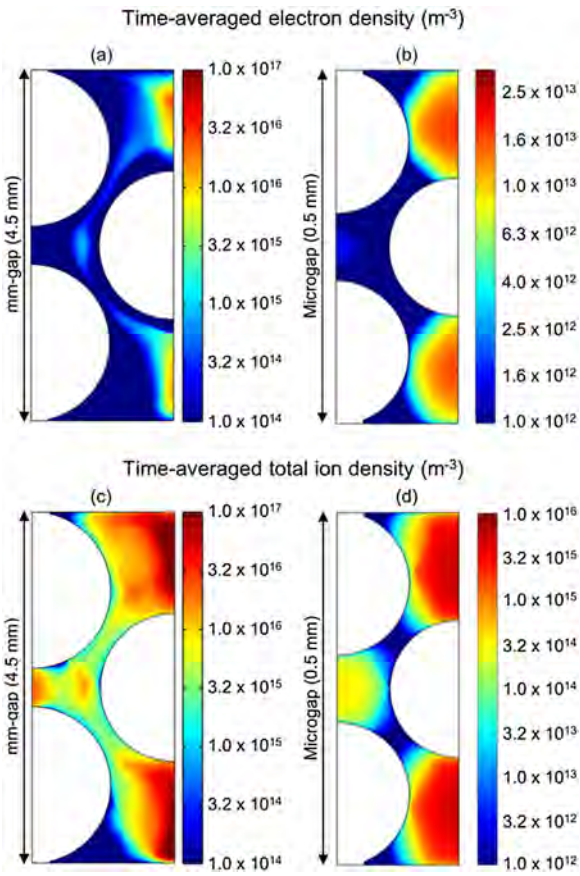

Figure 5. Time-averaged electron density (m^{-3}) and total ion density (m^{-3}) in the mm-gap (a and c) and microgap (b and d) reactors with a zirconia packing ($\varepsilon = 25$), for one cycle of applied potential. Note the difference in scale between the electron density and total ion density for the microgap reactor.

the boundaries, a strong density gradient exists in both cases. In the microgap reactor, due to the small dimensions, the plasma loses its quasi-neutrality (note the difference in electron and total ion densities in both legends). The fast electrons will accumulate on the dielectric surfaces, while the slower ions can stay longer in the void spaces. Nevertheless, also the maximum ion density is one order of magnitude lower than in the mm-gap reactor for the same applied potential, again due to more losses at the walls as a result of the smaller dimensions.

Furthermore, the combination of the enhanced electric field strength in the channels between the voids, which implies faster travelling electrons, and the smaller channel width itself, leads to the fact that in the channels between the voids in the microgap reactor, electrons are more likely to be absorbed at the walls. Indeed, the beads are too close to each other, and do not allow a high density of highly energetic electrons to exist in the channel between the voids, without them hitting (and charging) the walls, and thus, being removed from the gas gap. This explains

why no plasma exists in the channels in this case (for a dielectric constant of 25), as is clear from Figure 5(b and d). Our results can be linked to experimental observations by Ohsawa et al., who investigated the discharge characteristics of parallel electrodes with a disc of fused glass beads inside.[23] Their results showed that an increase in bead size implied a fewer number of current peaks with higher amplitude. Indeed, we also see less current peaks in the mm-gap reactor (with large beads) than in the microgap reactor. However, in our case the size of the gas gap and thickness of the dielectric layer do not stay constant, which explains why the amplitude will also increase for the microgap reactor. A thinner dielectric layer and smaller gap imply more power available, and therefore, stronger current peaks.

Thus, we can conclude that the discharge in the microgap and mm-gap packed bed DBD reactors is clearly different, with a higher electric field and electron temperature in the microgap reactor, leading to more current peaks per half-cycle, but also a lower plasma density and no quasi-neutral plasma in the voids between the beads, and even virtually no plasma formation in the channels between the voids, because of the smaller dimensions. However, also the dielectric constant of the packing has an influence on the discharge mechanism, which will be discussed in Section 3.2.

3.2. Influence of the Dielectric Constant of the Packing

We performed calculations for five different packing materials, with dielectric constants ranging from 5 (glass, quartz) over 9 (alumina), 25 (zirconia) and 100 (titania), up to 1000 (barium titanate). The dielectric constant of the dielectric layer covering the powered electrode was kept constant at 9 (alumina). In Figure 6 the time- and space-averaged electric field strength, electron temperature and electron density are plotted for both the microgap and the mm-gap as a function of dielectric constant. The electric field strength in the gas gap (Figure 6(a)) increases with the dielectric constant, which is expected. The higher the dielectric constant of the material, the stronger is the polarisation of the material, and thus, the greater is the difference between opposite charges at the contact points between the packing and the dielectric layer, and between two packing beads. For the mm-gap reactor, the electric field strength increases gradually with rising dielectric constant until $\varepsilon = 100$, while a further increase in dielectric constant does not result in a further enhancement of the electric field. This phenomenon was first reported by Chen et al. based on an approximative equation describing the electric field in a spherical void developed by Takaki et al.[14,24] The authors claimed that the enhancement of the electric field stagnates after a dielectric

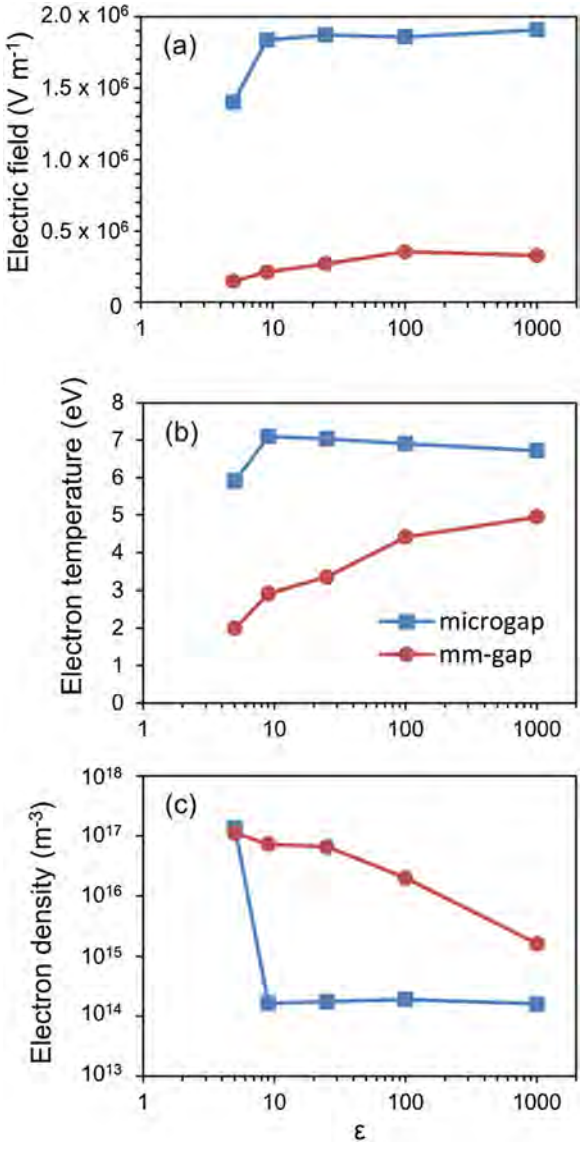

Figure 6. Influence of the dielectric constant on the space- and time-averaged electric field strength, electron temperature and electron density, for both the microgap (squares) and the mm-gap (circles) reactor.

constant of around 100, in correlation with our results for the mm-gap reactor. Mei et al. found comparable results in their experimental study on the conversion of CO_2 in a DBD filled with either glass beads, $BaTiO_3$ beads or no beads at all.[9] At a constant applied power, the average electric field strength increased when the glass packing was replaced with $BaTiO_3$ beads. Note that the applied potential was not constant in their study, due to the use of a power-driven source.

In the microgap reactor, on the other hand, the electric field strength only rises as a function of dielectric constant between $\varepsilon = 5$ and $\varepsilon = 9$, while larger dielectric constants do

not result in a further enhancement of the electric field. The increase in electric field strength from $\varepsilon = 5$ to $\varepsilon = 9$ can be explained as follows. When the dielectric constant of the packing material ($\varepsilon = 5$) is lower than the dielectric constant of the dielectric layer ($\varepsilon = 9$), the strongest polarisation of material takes place near the contact point between the dielectric layer and the upper packing bead. Therefore, the electric field is mainly enhanced at this contact point, but it is only very slightly enhanced in the rest of the reactor, like in the channels where the beads are the closest to each other; see Figure 7(a). As a result, the overall (space- and time-averaged) electric field will be much lower at $\varepsilon = 5$, compared to dielectric constants equal to or higher than the dielectric constant of the dielectric layer, where the polarisation is also rather strong in the rest of the reactor. This lower electric field will even affect the mechanism of the discharge, which will be explained a bit further.

Increasing the dielectric constant from $\varepsilon = 9$ to higher values again results in a more pronounced enhancement

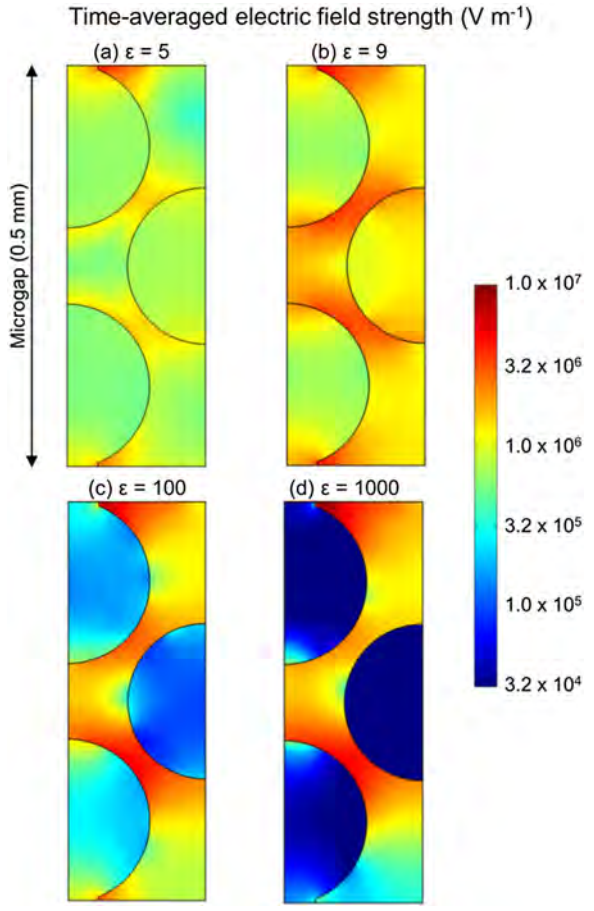

Figure 7. Time-averaged electric field strength in the microgap reactor for different packing materials: $\varepsilon = 5$ (a), 9 (b), 100 (c) and 1000 (d), for one cycle of applied potential. The electric field strength for $\varepsilon = 25$ was illustrated in Figure 3 (b) above.

of the electric field at the top contact point than at the bottom contact point with the grounded electrode, which is shown in Figure 7.

This can again be explained by means of the polarisation, and is a direct result from the fact that we consider a DBD reactor with only one dielectric barrier. Indeed, the difference in charge will always be lower between a charged and uncharged surface (i.e. ground electrode) than between two oppositely charged surfaces. As the dielectric constant of the packing material increases, this effect becomes more pronounced (see Figure 7(c and d)). Due to the small dimensions in the microgap reactor, the electric field in the two channels where the beads are closest will also be affected. The strong electric field at the top contact point, which is spread out quite far due to the small void spaces, will have a lowering effect on the electric field in the top channel. As a result, the electric field in the lower channel will be enhanced. However, the electric field enhancement near the grounded electrode is very limited (see Figure 7(c and d)). Therefore, the overall (space- and time-averaged) electric field strength will remain more or less constant upon increasing dielectric constant.

The space- and time-averaged electric field strength in general is more than an order of magnitude higher in the microgap reactor than in the mm-gap reactor (see Figure 6(a)), which is expected because the same potential difference is applied over a much smaller distance, so the delivered power per unit of distance is much higher in the microgap reactor. On the other hand, if we compare in both cases the value of the highest and the lowest electric field strength obtained, it is clear that the difference is larger in the mm-gap reactor. Indeed, the mm-gap reactor has an enhancement factor (i.e. ratio of highest and lowest electric field) of 2.4, i.e. $3.54 \times 10^5\,\mathrm{V\,m^{-1}}$ (at $\varepsilon = 100$) versus $1.48 \times 10^5\,\mathrm{V\,m^{-1}}$ (at $\varepsilon = 5$), while the enhancement factor in the microgap reactor is only 1.4, i.e. $1.91 \times 10^6\,\mathrm{V\,m^{-1}}$ (at $\varepsilon = 1000$) versus $1.40 \times 10^6\,\mathrm{V\,m^{-1}}$ (at $\varepsilon = 5$). In other words, our model predicts that the influence of changing the packing material on the electric field strength will be larger for the larger gap size. It would be nice if the effect of the dielectric constant on the electric field could also be measured experimentally in a mm-gap versus microgap set up, to validate our model predictions.

The electron temperature in Figure 6(b) follows the same trend as the electric field strength, with a few minor differences. For the mm-gap reactor, the electron temperature increases gradually upon rising dielectric constant, up to $\varepsilon = 1000$, while for the microgap reactor, the electron temperature decreases slightly above a dielectric constant of 9, instead of remaining more or less the same, like for the electric field strength. As discussed before, when the dielectric constant rises, the electric field strength is more enhanced at the top contact point than at the bottom contact point with the grounded electrode. The influence on

the overall electric field strength is rather small, but the effect is much more pronounced on the electron temperature. Indeed, because the electrons cannot be accelerated to the same extent in the bottom part of the reactor, the overall electron temperature slightly decreases with increasing dielectric constant. For the mm-gap reactor this phenomenon also takes place, but because of the larger dimensions it does not have the same impact. Here, the enhancement in the top part of the reactor has a larger influence on the electron temperature than the reduced effect in the bottom part, which explains why the space- and time-averaged electron temperature gradually increases upon rising dielectric constant, even between $\varepsilon = 100$ and 1000, where the electric field strength has saturated.

The electron temperature is again lower in the mm-gap reactor than in the microgap reactor, due to the lower electric field strength, but because it keeps on rising with increasing dielectric constant, it is a factor 3 lower than in the microgap reactor for $\varepsilon = 5$, while it is only a factor 1.4 lower for $\varepsilon = 1000$. This suggests that the advantage of a microgap reactor, in terms of enhanced electric field and electron temperature, is more prominent for packing materials with smaller dielectric constants, but is obviously reduced for packing materials with larger dielectric constants. The trend in the mm-gap is consistent with the results found by Mei et al.[9] Again, it would be nice if more experiments could be performed for a microgap reactor, so that the calculated trends could be verified in more detail.

The electron density in Figure 6(c) shows the opposite behaviour than the electric field strength, because it drops upon increasing dielectric constant. The stronger the electric field, the lower is the electron density and vice-versa. Indeed, a stronger electric field strength implies faster travelling electrons, and thus, more collisions with the walls, removing the electrons from the gas gap and charging the surfaces. At $\varepsilon = 5$, the space- and time-averaged electron density is roughly the same for both the microgap and mm-gap reactor. For the mm-gap reactor, the electron density drops only slightly from $\varepsilon = 5$ to $\varepsilon = 25$ but then it drops a factor 40 from $\varepsilon = 25$ to $\varepsilon = 1000$. On the other hand, for the microgap reactor, a drop in electron density by three orders of magnitude is observed, when increasing the dielectric constant from 5 to 9, while for higher dielectric constants, the electron density stays more or less constant. At $\varepsilon = 1000$, the space- and time-averaged electron density in the microgap reactor is about one order of magnitude lower than in the mm-gap reactor.

The reason of the significant drop in electron density upon increasing dielectric constant, i.e. between $\varepsilon = 25$ and 1000 in the mm-gap reactor, and between $\varepsilon = 5$ and 9 in the microgap reactor, can be explained from the fact that the discharge behaviour changes significantly within this range of dielectric constants. Indeed, in the mm-gap reactor, when the dielectric constant rises from 25 to 100, the plasma cannot flow anymore through the channels between the voids, as is clear from Figure 8. The discharges preferably take place above and below the right packing bead and in between the two packing beads on the left. The reason is that the electric field enhancement becomes too strong in the channels between the voids, accelerating the electrons so that they get more easily absorbed at the beads. The overall plasma volume will thus be lower, which results in a lower overall (space- and time-averaged) electron density, as shown in Figure 6(c). Further increasing the dielectric constant to 1000 will shift the electric field enhancement to the top part of the reactor, very similar to what happens in the microgap reactor already at lower dielectric constants of $\varepsilon = 25$, as discussed before. As a result, no plasma will be formed anymore between the bead on the right and the grounded electrode (cf. Figure 8), resulting in an even lower overall electron density.

For the microgap reactor, the strong drop in space- and time-averaged electron density from $\varepsilon = 5$ to $\varepsilon = 9$ can be explained because the plasma behaviour at $\varepsilon = 5$ is quite different from the behaviour at higher dielectric constants (cf. the behaviour for $\varepsilon = 25$ discussed before). When $\varepsilon = 5$, and thus, lower than the value of the dielectric layer, the plasma gains the ability to flow through the channels between the voids, because the electric field strength will not be as strongly enhanced in the channels between the voids than at higher dielectric constants. Instead of the multiple current peaks as seen in Figure 2(b), the current profile will now only contain two very strong current peaks per half cycle, arising from two consecutive discharges flowing through the channel of voids, as shown in Figure 9. The full gas gap can be filled with plasma, resulting in a much higher overall electron density. At higher dielectric constants, even at $\varepsilon = 9$, this is not possible anymore, as

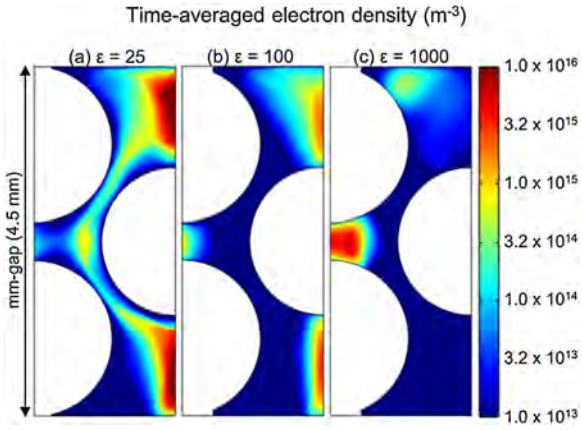

Figure 8. Time-averaged electron density in the mm-gap reactor for three different packing materials: $\varepsilon = 25$ (a), 100 (b) and 1000 (c), for one cycle of applied potential.

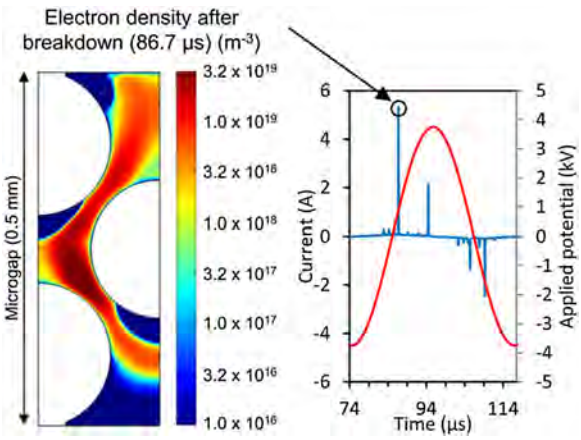

Figure 9. Electron density profile in the microgap reactor with glass beads ($\varepsilon = 5$), immediately after the breakdown at 86.7 μs.

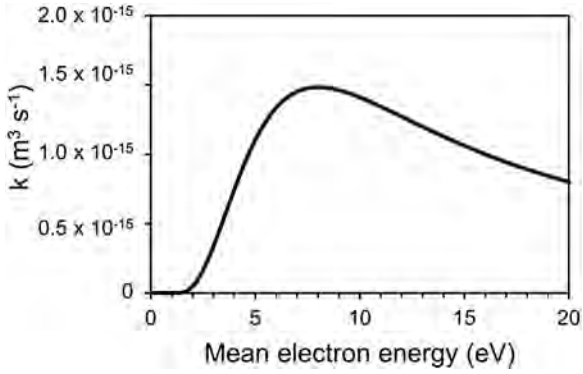

Figure 10. Reaction rate constant for the dissociation of CO_2 as a function of mean electron energy.

discussed before, explaining the strong drop in space- and time-averaged electron density, illustrated in Figure 6(c).

To summarise, upon increasing dielectric constant, the electric field strength is more enhanced at the contact points between dielectric materials or in places where these materials are close to each other. However, since we are studying a DBD reactor with only one dielectric barrier, the electric field enhancement, and thus, the ability to cause a breakdown will become lower near the grounded electrode, which is not covered by a dielectric layer, upon increasing dielectric constant of the packing. At low dielectric constant of the packing, when the polarisation, and thus, the electric field enhancement is somewhat more limited, the discharge can more easily flow through the channels between the voids. However, at higher dielectric constants, the plasma loses this ability and ultimately shifts to the top part of the reactor, away from the grounded electrode. When the dimensions of the reactor are smaller, the influence of an increase in dielectric constant is much more pronounced, causing the plasma to change its behaviour much earlier, namely already between $\varepsilon = 5$ and 9.

To answer the question whether a smaller packed bed DBD reactor will eventually be better for use in environmental applications like CO_2 splitting, we combine our calculated mean electron energy and electron density data at every mesh point and at every time step with a look-up table for the electron impact dissociation rate constant of CO_2 as a function of mean electron energy, in order to estimate the CO_2 dissociation rate. Figure 10 gives a visual representation of this look-up table. The dissociation rate constant is obtained from the cross section of electron impact excitation of CO_2 with a threshold of 7 eV, representing the most probable pathway for dissociation via an electronic excited state.[25–28] The look-up table as a function of mean electron energy is generated with Bolsig+, a software program solving the Boltzmann equation for the electrons, using the input collision cross sections from the Phelps database on LXcat.[29,30] The space- and time-averaged electron impact dissociation rate calculated in this way is plotted in Figure 11 as a function of the dielectric constant of the packing, for both the mm-gap and microgap reactor.

In the mm-gap reactor, a packing with higher dielectric constant will increase the electric field strength and electron temperature (see Figure 6(a and b)), and therefore, also the electron impact dissociation rate constant, resulting in a rise in the dissociation rate (see Figure 11). However, above a dielectric constant of 25, the drop in electron density becomes significant (see Figure 6(c)), and thus, in spite of the increasing rate constant, the CO_2 dissociation rate will slightly drop again. This result does not correlate to the results obtained by Mei et al., who reported an increase in CO_2 conversion when the glass ($\varepsilon = 5$) beads were replaced with $BaTiO_3$ ($\varepsilon = 1000$).[9] The drop in CO_2 dissociation rate in our case is caused by the severe drop in electron density. The conditions studied by Mei et al.[9] are

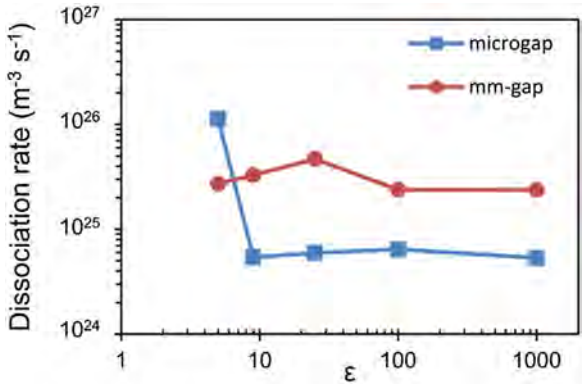

Figure 11. Influence of the dielectric constant on the space- and time-averaged electron impact dissociation rate of CO_2, for both the microgap and the mm-gap reactor.

however, not exactly the same, and it might be that at their conditions, the drop in electron density is not so severe. As no electron densities were reported by Mei et al.,[9] it is difficult to know the exact underlying reason. On the other hand, it might also be that our estimation of the CO_2 dissociation rate, as explained before, is too approximate, because it is calculated from discharge parameters for a helium plasma. Moreover, the discharge in our model is considered homogeneous, which is correct for a helium plasma, but in CO_2 it will be a combination of local surface and filamentary discharges. Therefore, we have to be careful with drawing conclusions from this simple estimation. Finally, the model only focuses on the differences in the dielectric constant, while in reality there will be more differences between the $BaTiO_3$ and glass beads, which might explain the higher CO_2 conversion when using the $BaTiO_3$ beads.

The calculated CO_2 dissociation rate in the microgap reactor follows almost perfectly the trend of the calculated electron density; cf. Figures 11 and 6(c). The higher electric field strength and electron temperature when increasing ε from 5 to 9 is too limited to compensate for the strong drop in overall electron density. The resulting dissociation rate therefore, drops by a factor 20. Overall, this simplified calculation predicts that the microgap packed bed DBD reactor shows a higher dissociation rate than the mm-gap reactor, in case of glass packing beads ($\varepsilon = 5$). Indeed, at these conditions the electron density is still comparable to the mm-gap reactor, but the mean energy is much higher, giving rise to a higher dissociation rate. For packing materials with higher dielectric constant, the microgap packed bed DBD reactor seems to result in a much lower CO_2 dissociation rate than a mm-gap reactor, due to the significant drop in electron density.

To conclude, our calculations (with these specific input parameters) reveal that using a packing with higher dielectric constant only seems to make sense in a reactor with a large gap. However, our model predicts that even in a mm-gap reactor, after a certain value the beneficial effects of electric field enhancement will be countered by the drop in electron density. In a microgap reactor, the electron density seems to be the most important parameter in determining the CO_2 dissociation rate, so our calculations predict that in this case a packing with lower dielectric constant will be beneficial.

Currently, we are performing experiments to investigate the CO_2 dissociation in both a mm-gap and microgap reactor for different packing materials, and the first preliminary results seem to indicate similar trends. However, the different packing materials in the experiments do not only have different dielectric constants, but they might also have other characteristics, like the morphology, porosity and chemical activity (acid-base properties), etc, which can also affect the outcome.[8,20] Hence, this shows the added value of modelling, where the effect of one separate parameter, i.e. here the dielectric constant, can be investigated.

4. Conclusion

We studied the influence of the gap size and the dielectric constant of various packing materials on the plasma characteristics in a packed bed DBD reactor, by means of fluid modelling. A 2D axisymmetric model was developed for both a mm-gap and a microgap packed bed DBD reactor. The plasma behaviour is significantly different for a mm-gap reactor and a microgap reactor, when applying the same potential. Due to the small dimensions, the electric field strength is more enhanced in a microgap reactor, resulting in more current peaks per half cycle, because the electric field strength needed to cause a breakdown, is more often reached. On the other hand, the small dimensions and enhanced electric field in the microgap reactor will cause the plasma to lose its quasi-neutrality, because the electrons get easily lost at the walls and the surface of the packing beads. For the same reason, the ion density is also clearly lower in the microgap reactor than in the mm-gap reactor, and the plasma is not able to flow through the channels between the voids, except for very low dielectric constants.

In both the microgap and mm-gap reactor, using a packing with higher dielectric constant increases the electric field strength, but only up to a certain extent. For the mm-gap reactor the electric field increases up to $\varepsilon = 100$ after which it stagnates. For the microgap reactor, the electric field does not increase anymore above a dielectric constant of 9. Further increasing the dielectric constant will cause the electric field enhancement to take place only at the top part of the reactor, leaving a lower electric field strength near the bottom, where there is less polarisation between the lower bead and the grounded electrode. However, the overall (space- and time-averaged) electric field is not really affected by this behaviour, and stays more or less the same from $\varepsilon = 9$ to 1000.

The effect on the electron temperature is very similar. In the mm-gap reactor an enhanced electric field upon increasing dielectric constant of the packing results in a higher electron temperature. In the microgap reactor the electron temperature also increases but again only up till $\varepsilon = 9$. The slight decrease afterwards is attributed to the fact that the electric field enhancement mainly takes place at the top part of the reactor.

Finally, the electron density follows more or less the opposite trend as the electric field, with a significant drop between $\varepsilon = 5$ and 9 for the microgap reactor, and a similar drop between $\varepsilon = 25$ and 1000 for the mm-gap reactor, which is attributed to a change in discharge mechanism. For

the mm-gap reactor, the plasma loses the ability to travel through the channels between the voids when ε rises from 25 to 1000, resulting in an overall lower electron density. The same behaviour takes place in the microgap reactor, but in this case, even at a dielectric constant of 9, the plasma cannot flow through the channels, and only when ε drops to 5, the plasma gains the ability to travel through the gaps, changing the discharge behaviour, and resulting in a much higher overall electron density than for the higher dielectric constants.

By coupling our calculated mean electron energy and electron density values with a look-up table for the reaction rate of electron impact CO_2 dissociation, we predict that for the mm-gap reactor the CO_2 dissociation rate tends to increase with rising dielectric constant of the packing beads, following the trend of the electric field and electron temperature, but above a certain dielectric constant (i.e. $\varepsilon = 25$ for a gap size of 4.5 mm), the beneficial effects of the electric field enhancement will be countered by the drop in electron density. For the microgap reactor, the electron density is obviously the dominant factor. Regardless of the higher electric field strength, the electron impact dissociation rate of CO_2 will drop upon rising dielectric constant of the packing beads from $\varepsilon = 5$ to $\varepsilon = 9$, because of the significant drop in electron density. Therefore, our calculations reveal that using a packing with higher dielectric constant, at these input parameters, only makes sense when the gap is large (in the order of millimetres). In a microgap (less than 1 mm) reactor, a packing with a low dielectric constant seems to give the best results. We hope to validate these model predictions with experiments in the near future.

Acknowledgements: This research was carried out in the framework of the network on Physical Chemistry of Plasma-Surface Interactions – Interuniversity Attraction Poles, phase VII (http://psi-iap7.ulb.ac.be/), and supported by the Belgian Science Policy Office (BELSPO). K. Van Laer is indebted to the Institute for the Promotion of Innovation by Science and Technology in Flanders (IWT Flanders) for financial support. The calculations were carried out using the Turing HPC infrastructure at the CalcUA core facility of the Universiteit Antwerpen (UAntwerpen), a division of the Flemish Supercomputer Center VSC, funded by the Hercules Foundation, the Flemish Government (department EWI) and the UAntwerpen.

Received: July 6, 2016; Revised: September 7, 2016; Accepted: September 11, 2016; DOI: 10.1002/ppap.201600129

Keywords: dielectric barrier discharge; fluid modelling; packed bed; packing effect; plasma

[1] K. Schmidt-Szalowski, A. Borucka, *Plasma Chem. Plasma Proc.* **1989**, *9*, 235.
[2] S. Jodzis, *Ozone-Sci. Eng.* **2003**, *25*, 63.
[3] H. L. Chen, H. M. Lee, M. B. Chang, *Ozone: Sci. Eng.* **2006**, *28*, 111.
[4] C. L. Chang, T. S. Lin, *Plasma Chem. Plasma Proc.* **2005**, *25*, 227.
[5] H. X. Ding, A. M. Zhu, X. F. Yang, C. H. Li, Y. Xu, *J. Phys. D: Appl. Phys.* **2005**, *38*, 4160.
[6] M. Kraus, B. Eliasson, U. Kogelschatz, A. Wonkaun, *Phys. Chem. Chem. Phys.* **2001**, *3*, 294.
[7] H. L. Chen, H. M. Lee, S. H. Chen, Y. Chao, M. B. Chang, *Appl. Catal. B: Environ.* **2008**, *85*, 1.
[8] Q. Yu, M. Kong, T. Liu, J. Fei, X. Zheng, *Plasma Chem. Plasma Process.* **2012**, *32*, 153.
[9] D. Mei, X. Zhu, Y. He, J. D. Yan, X. Tu, *Plasma Sources Sci. Technol.* **2015**, *24*, 015011.
[10] K. Van Laer, A. Bogaerts, *Energy Technol.* **2015**, *3*, 1038.
[11] E. C. Neyts, A. Bogaerts, *J. Phys. D: Appl. Phys.* **2014**, *47*, 224010.
[12] E. C. Neyts, K. Ostrikov, M. K. Sunkara, A. Bogaerts, *Chem. Rev.* **2015**, *115*, 13408.
[13] J. S. Chang, K. G. Kostov, K. Urashima, T. Yamamoto, Y. Okayasu, T. Kato, T. Iwaizumi, K. Yoshimura, *IEEE Trans. Ind. Appl.* **2000**, *36*, 1251.
[14] K. Takaki, J. S. Chang, K. G. Kostov, *IEEE Trans. Dielectr. Electr. Insul.* **2004**, *11*, 481.
[15] W. S. Kang, J. M. Park, Y. Kim, S. H. Hong, *IEEE Trans. Plasma Sci.* **2003**, *31*, 504.
[16] H. Russ, M. Neiger, J. E. Lang, *IEEE Trans. Plasma Sci.* **1999**, *27*, 38.
[17] N. Y. Babaeva, M. J. Kushner, *Plasma Sources Sci. Technol.* **2009**, *18*, 035009.
[18] Y. Zhang, H. Wang, W. Jiang, A. Bogaerts, *New J. Phys.* **2015**, *17*, 083056.
[19] K. Van Laer, A. Bogaerts, *Plasma Sources Sci. Technol.* **2016**, *25*, 015002.
[20] X. Duan, Z. Hu, Y. Li, B. Wang, *AIChE J.* **2015**, *61*, 898.
[21] B. Wang, W. Yan, W. Ge, X. Duan, *Chem. Eng. J.* **2013**, *234*, 354.
[22] http://www.comsol.com.
[23] A. Ohsawa, R. Morrow, A. B. Murphy, *J. Phys. D: Appl. Phys.* **2000**, *33*, 1487.
[24] H. L. Chen, H. M. Lee, S. H. Chen, M. B. Chang, *Ind. Eng. Chem. Res.* **2008**, *47*, 2122.
[25] L. D. Pietanza, G. Colonna, G. D'Ammando, A. Laricchiuta, M. Capitelli, *Plasma Sources Sci. Technol.* **2015**, *24*, 042002.
[26] L. D. Pietanza, G. Colonna, G. D'Ammando, A. Laricchiuta, M. Capitelli, *Phys. Plasmas* **2016**, *23*, 013515.
[27] L. D. Pietanza, G. Colonna, G. D'Ammando, A. Laricchiuta, M. Capitelli, *Chem. Phys.* **2016**, *468*, 44.
[28] A. Bogaerts, W. Wang, A. Berthelot, V. Guerra, *Plasma Sources Sci. Techhol.* **2016**, *25*, 055016.
[29] G. J. M. Hagelaar, L. C. Pitchford, *Plasma Sources Sci. Technol.* **2005**, *14*, 722.
[30] Phelps Database, www.lxcat.net retrieved on June 28, 2016.